Journal of Materials Chemistry A

ROYAL SOCIETY OF CHEMISTRY

PAPER

View Article Online
View Journal | View Issue

Cite this: J. Mater. Chem. A, 2024, 12, 5233

Photochemical transformation of a perylene diimide derivative beneficial for the *in situ* formation of a molecular photocatalyst of the hydrogen evolution reaction†

Estera Hoffman,[a] Karol Kozakiewicz,[ab] Małgorzata Rybczyńska,[ab] Michał Mońka,[a] Daria Grzywacz,[ab] Beata Liberek,[b] Piotr Bojarski[a] and Illia E. Serdiuk *[a]

The photocatalytic splitting of water gains more and more attention as one of the most promising environmentally friendly approaches for the production of green hydrogen fuels. In this article, we report a peculiar feature of a carbazole derivative of the perylene diimide dye **Cbz-PDI** which forms in the presence of platinum salt and sunlight an efficient molecular photocatalyst of the hydrogen evolution reaction (HER). Such a photocatalyst (**Cbz-PDCA-Pt$_2$**) represents a unique group of organometallic platinum complexes with good sunlight absorption, satisfactory solubility, high stability and HER photoactivity. The *in situ* formation seems to be a convenient solution to the problems with the preparation, isolation and storage of such compounds. The best HER performance (in terms of the turnover number of 1900, decreased platinum usage and increased stability for longer than 3 days) was achieved when **Cbz-PDCA-Pt$_2$** formed a mixture with **Cbz-PDI** and the molar percentage of platinum in the mixture did not exceed 10%. In such a system, **Cbz-PDI** facilitates charge separation and the storage of excitation energy due to the long lifetimes of its excited states observed as a result of thermally activated delayed fluorescence (TADF). The discovered photoreactivity of the perylene diimide derivative can hopefully open a new direction in the organometallic materials for use in molecular (photo)catalysis.

Received 29th September 2023
Accepted 5th December 2023

DOI: 10.1039/d3ta05930h

rsc.li/materials-a

Introduction

Research towards alternative fuels gains increasing attention and efforts lately due to threatening climate changes on the one hand and decreasing stability of oil and gas markets on the other hand, requiring a concerted effort from humanity, specifically the scientific community. There is an urgent need for environmentally friendly, abundant and efficient energy sources. In response to global warming and the requirements of reduction of CO_2 emission, at least partial replacement of fossil fuels with hydrogen is regarded as one of the most promising solutions to be implemented in the near future.[1,2] In fact, from the viewpoint of combustion process, among other fuels, hydrogen affords the highest energy capacitance due to its minimal molecular weight and zero CO_2 emissions because the only product of the oxidation of pure H_2 is water. The key problem is how to produce "green" H_2, avoiding the use of fossil fuel energy at any stage of preparation, including electricity generated by the combustion of coal, oil or gas.

The photocatalytic splitting of water seems to be an elegant solution representing the direct transformation of sunlight energy to transportable chemical fuels, including H_2.[3–5] The application of photocatalysis for hydrogen evolution reaction (HER) from water is a promising approach that is still in the early stages of development. A growing number of investigations aiming to improve the parameters of the photocatalytic HER are driven by its potential to considerably increase the efficiency and decrease the costs of converting solar energy into H_2 as an alternative to the "green" H_2 obtained by electrolysis using electricity from photovoltaic cells.[6]

The light-induced HER requires a photocatalytic system, which can be of two types: heterogeneous or homogeneous. In the first type, the key processes such as light absorption, charge transport, and water reduction usually occur on separate fragments of the photocatalytic system: the photosensitizer, mediator and (co)catalyst, respectively.[7] These are the most intensively studied systems and have the highest state-of-the-art photocatalytic HER efficiencies and stabilities. In contrast, in a homogeneous system represented by a molecular photocatalyst, all these processes should occur in the same molecule. The achievement of a high efficiency of sunlight

[a]Faculty of Mathematics, Physics and Informatics, University of Gdańsk, Wita Stwosza 57, 80-308 Gdańsk, Poland. E-mail: illia.serdiuk@ug.edu.pl; Tel: +48 58 523 22 44
[b]Faculty of Chemistry, University of Gdańsk, Wita Stwosza 63, 80-308 Gdańsk, Poland

† Electronic supplementary information (ESI) available: It includes the synthetic procedures and results of analyses; the results of the DFT calculations, including the optimized structures, energies and molecular orbitals; and additional results from the spectroscopic measurements. See DOI: https://doi.org/10.1039/d3ta05930h

absorption and photocatalytic activity, together with long-term stability within a single molecular system, is extremely challenging, which explains the very limited number of molecular HER catalysts known to date, especially those applicable to photocatalysis. Nevertheless, the key advantage of homogeneous systems is their higher solubility and much lower aggregation in water. In the case of high stability, these factors can enable a sufficient number of active photocatalytic sites present in a limited solution volume, thus affording high power efficiency of photocatalytic HER and finally bringing us closer to the development of a respective "green" H_2 technology.

As compared to the heterogeneous photocatalytic systems, the homogeneous catalysts offer higher atom economy and selectivity of photoreaction, while their mechanistic investigations and analysis of their structure–property relationships are generally much easier. For these reasons, research on molecular catalysts like metalorganic complexes is one of topical directions of material science.

An ideal metalorganic complex for the photocatalytic HER reaction should have (i) strong sunlight absorption, (ii) an appropriate LUMO level above −4.4 eV (*vs.* vacuum) to enable water reduction, (iii) balanced hydrogen adsorption/desorption thermodynamics to enable high H_2 evolution and (iv) high photo- and mechanical stability. The organic ligand and its interactions with the metal have a crucial role in the modulation of parameters (i), (ii) and (iv). Recently developed molecular catalytic systems include various metal complexes with porphyrin and corrole ligands. Particularly, Co,[8] Ni[9] and Cu[10] complexes applied to the surface of an electrode show high stability and efficiency in the electrocatalytic HER tests. Other efficient electrocatalytic Ni complexes include various diazadiphosphacyclooctane[11] and azadiphosphacycloheptane[12] derivatives as stable and strongly binding ligands.

From the point of view of HER thermodynamics, platinum has the most suitable electronic configuration and presents at the maximum of the volcano plot,[13] binding neither too strongly nor too weakly to a substrate (H_2O or H_3O^+) and product (H and H_2). Its superior catalytic properties are usually realized in heterogeneous catalytic systems, which use it in the form of colloids, nanoparticles or alloys.[14] Such approaches, however, waste considerable amounts of this precious metal beneath the active surface and have considerable problems with mechanical stability (*e.g.* the aggregation of (nano)particles), decreasing the active surface area. To form a homogeneous complex, Pt is chelated with various aliphatic amines and their derivatives as ligands.[15]

In spite of excellent electrocatalytic performance, the abovementioned Pt complexes rarely catalyze the photoinduced HER. For the latter purpose, molecular catalysts are usually incorporated onto the surface of a (semi)conductor (*e.g.* TiO_2,[16] graphene derivatives[17,18] or metal colloids[19]) to give a heterogeneous system. Naturally occurring [Fe–Fe]-hydrogenase[20] can serve as one of the rare examples of a water-soluble HER photocatalyst with medium-to-low efficiency.

In spite of the fact that platinum complexes seem to be a route to the most efficient and relatively economic "green" H_2 production, examples of their use in the role of photocatalyst itself are surprisingly scarce.[21] A few reported examples include Pt complexes with Schiff bases, although there is evidence of considerable problems with photostability, HER efficiency[22] and solubility in aqueous solutions.[23] The nature of the ligand (*e.g.* its chelating ability and light absorptivity) seems to be important in functional metalorganic materials with Pt. Moreover, synthesis of such complexes requires specific equipment and storage conditions due to the sensitivity of Pt precursors towards light, oxidation and other reactions.

In response to the high demand for efficient photocatalysts of the HER, in this article we report the remarkable ability of a perylene diimide derivative to undergo photochemical activation to a ligand that forms a stable molecular platinum complex. This Pt complex can act as an efficient photocatalyst of the HER. As a result, a convenient method for the *in situ* preparation of a highly stable Pt complex **Cbz-PDCA-Pt$_2$** (Fig. 1) with photocatalytic activity is described. The ligand fragment responsible for the absorption of light is formed *via* the irradiation of 1,7-bis[4-(carbazol-9-yl)phenyl]-*N*,*N*-bis(2-ethylhexyl)perylene-3,4:9,10-tetracarboxylic acid diimide (**Cbz-PDI**, Fig. 1) with sunlight, which, in the presence of the platinum salt, forms **Cbz-PDCA-Pt$_2$**. The molecular design of the ligand presented here applies the electron donor–acceptor molecular architecture, photoreactive sites and alkyl groups that prevent aggregation and improve solubility.

Perylene diimide was selected as an electron acceptor fragment with good sunlight absorption and which, as we discovered, forms complexes with Pt under irradiation. Moreover, perylene itself shows good semiconductor properties and a high (photo)chemical stability. Carbazole was selected as a (photo) chemically stable and bulky electron donor which enables the formation of a charge transfer (CT) state under excitation yet preserving reasonable light absorption, and provides partial separation of the frontier orbitals to facilitate charge separation. The designed **Cbz-PDCA-Pt$_2$** molecule undergoes more than 1000 turnovers of the HER in 24 h under sunlight irradiation in the presence of sacrificial electron donors and remains active for more than 3 days. The unique photochemical transformation of a perylene diimide fragment, affording a strong chelating ligand under the conditions of the HER, is a new approach in the development of homogeneous HER photocatalysts.

Results and discussion

Preparation of Cbz-PDI

The precursor of the ligand, **Cbz-PDI**, was prepared in a two-step reaction *via* a modified procedure.[24] Briefly, 1,7-dibromoperylene-3,4,9,10-tetracarboxylic dianhydride reacted with 2-ethylhexyl amine and further with 4-[(carbazol-9-yl)phenyl] boronic acid in a Suzuki coupling to give **Cbz-PDI** in a 65% yield. The details of the synthetic procedures and analyses are provided in the ESI (Fig. S1 and S2).†

Spectral properties and changes during the formation of the Pt complex

Due to the specific interest in the light absorption properties and their changes during the photochemical formation of the Pt complex, the origin of the electronic transitions in **Cbz-PDI** and related perylene derivatives is discussed in detail.

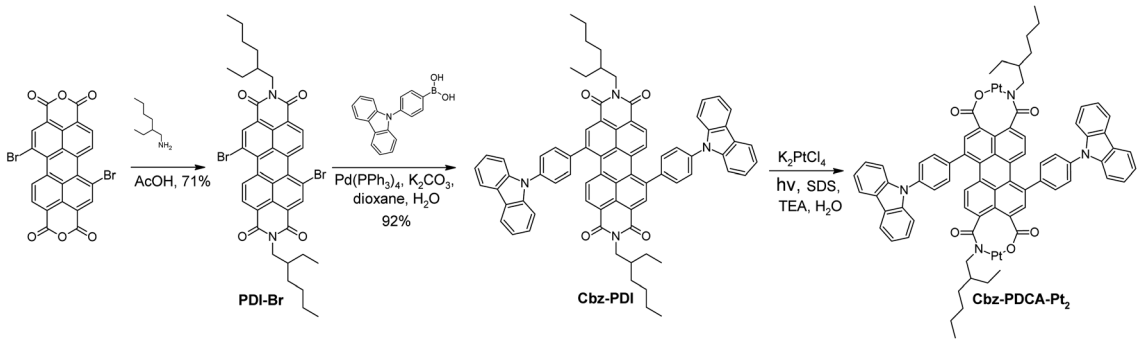

Fig. 1 Synthesis of **Cbz-PDI** and **Cbz-PDCA-Pt$_2$**.

Cbz-PDI shows a broad absorption covering almost all of the visible region from 380 to 650 nm. This originates mainly from two key electronic transitions: a low-energy charge transfer (CT) transition involving an *N*-phenylcarbazole donor and a PDI acceptor and a locally excited (LE) transition within the PDI acceptor fragment (Fig. S3, ESI†). Typically, the CT transition appears as a broad band with absorption centered at 540 nm (Fig. 2A, Table 1). The respective CT fluorescence band is specifically sensitive to medium polarity, namely shifting by 0.23 eV (100 nm) from cyclohexane to chloroform solutions (Fig. 2B, Table 1). The LE transition has a higher energy: its absorption maximum appears near 500 nm in **Cbz-PDI** and free PDI acceptor. The respective LE fluorescence can be observed in solutions of PDI, with a maximum near 530 nm. In the view of the following discussion, it is important to mention that the LE energy increases when the cyclic amide fragment is absent. In fact in the perylene parent molecule, the absorption and fluorescence maxima appear at 440 nm and 445 nm, respectively. This indicates that the conjugation of the perylene core with the carboxyl amide groups regulates the stabilization of the LE transition and structural changes in this fragment are reflected in the electronic spectra.

When an aqueous solution of **Cbz-PDI** is irradiated by sunlight in the presence of triethylamine (TEA, 0.3 M), K_2PtCl_4 (50 μM) and sodium dodecyl sulphate (2.1 mM), referred further as activation, its color changes from bright violet to dark yellow and the absorption spectra undergo strong changes (Fig. 3A). Within the first hour of irradiation, the 545 nm band shifts to one at 500 nm with a complex structure and a band centered at 750 nm appears. Further irradiation leads to a shift of the 500 nm band to 450 nm. The 750 nm band disappears, most likely indicating the formation and deactivation of the radical anion species of **Cbz-PDI**, formed as a result of the quenching of its excited state by TEA. This mixture produces hydrogen, as shown in Fig. 3B. During the first hour of irradiation, minimal amounts of H_2 are produced, but after 2–3 h, the TOF value reaches its maximum of 30 mol H_2 per 1 mol of Pt for 1 h and then remains stable. Reaching the TOF maximum correlates with the maximum contribution of the 450 nm band in the absorption spectra. This indicates that species with this absorption are responsible for the HER activity of the investigated system.

In an attempt to reveal the key activation steps and structural components of these species, we performed various HER tests under different conditions. It was found that under irradiation in the absence of K_2PtCl_4, the mixture did not produce H_2, whereas the appearance of 450 nm band was not observed in the absorption spectra. The same lack of activation was observed when TEA was replaced by ascorbic acid (AA), an acidic sacrificial electron donor. The activated species were thus formed under basic conditions and contained Pt.

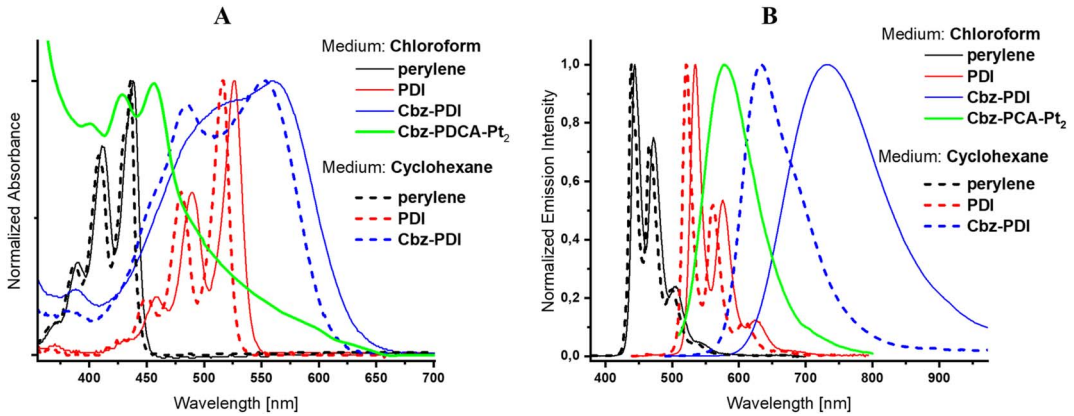

Fig. 2 Absorption (A) and fluorescence (B) spectra of **Cbz-PDI** before and after activation, PDI, and perylene in chloroform and cyclohexane.

Table 1 Absorption and emission maxima of perylene, PDI and **Cbz-PDI** before and after (**Cbz-PDCA-Pt$_2$**) activation in aprotic solvents

Compound	Medium	λ_{abs} [nm]	λ_{em} [nm]
Perylene	Cyclohexane	435	440
	Chloroform	440	445
PDI	Cyclohexane	515	520
	Chloroform	525	535
Cbz-PDI	Cyclohexane	550	630
	Chloroform	560	730
Cbz-PDCA-Pt$_2$	Chloroform	450	580

As compared to **Cbz-PDI**, the absorption of the activated mixture lacks the CT band centered at 540 nm, indicating a significant decrease in the strength of acceptor or donor. The LE absorption maximum is higher than that of the PDI acceptor, but lower than that of perylene. Considering the high stability of the carbazole donor under the applied conditions and importance of basic conditions for the activation process, we conclude that the irradiation of **Cbz-PDI** facilitated the gradual hydrolysis of the cyclic diimide of the PDI fragment, decreasing its electron acceptor properties. The nucleophilic attack of hydroxyl anions can lead to the opening of the diimide ring with the formation of a chelate

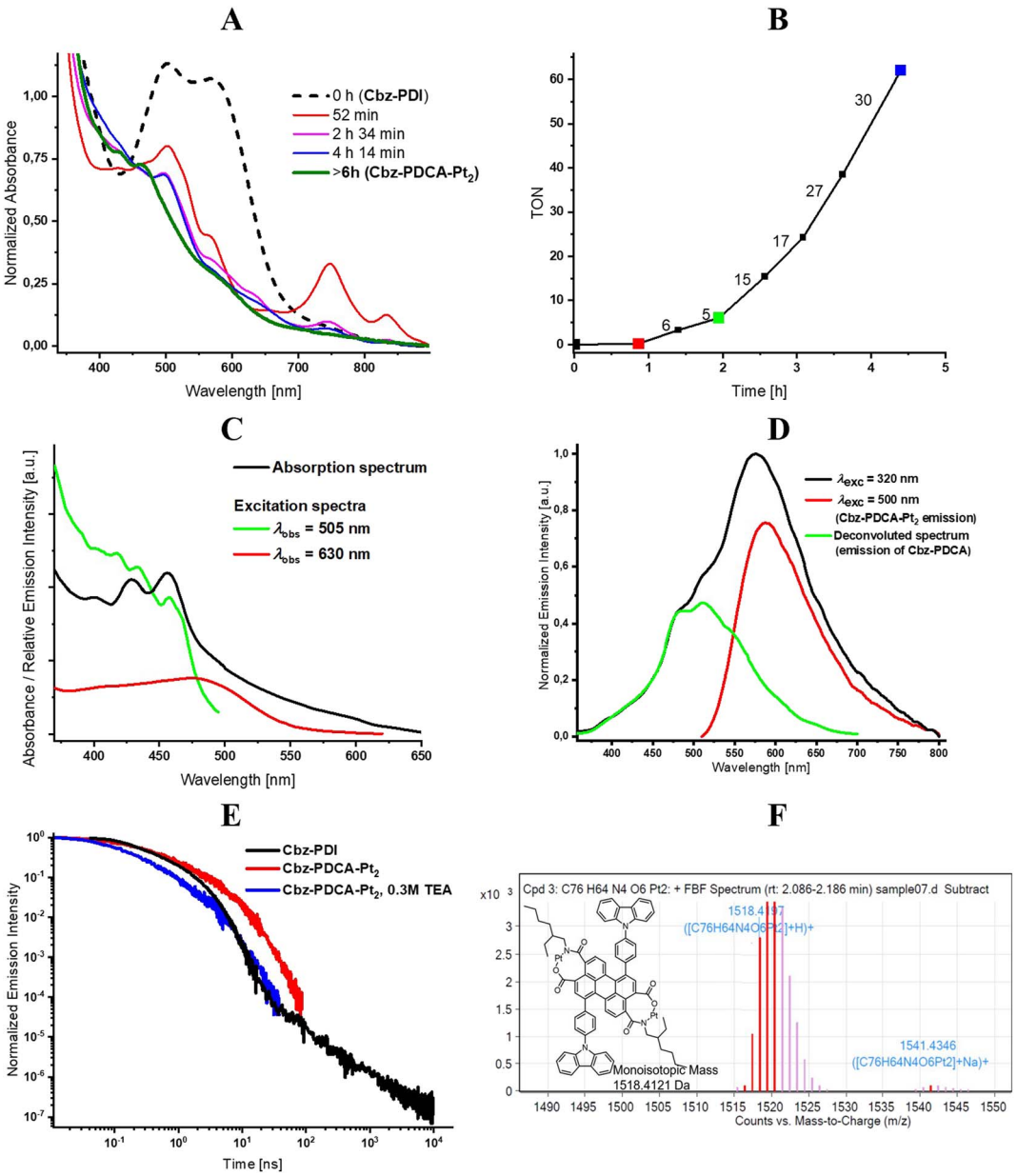

Fig. 3 Changes in the absorption spectra (A) and contamination of H_2 in the gaseous phase (B) during the activation of **Cbz-PDI**; the numbers on the plot indicate the TOF values; TON is calculated per mole of K_2PtCl_4. Fluorescence excitation (C) and emission (D) spectra, emission decay (E) and mass spectrum (F) of the activated mixture containing **Cbz-PCA-Pt$_2$**.

fragment consisting of an *N*-(2-ethylhexyl)carboxamide group in the vicinity of a carboxylate anion. Such a chelate fragment can form a complex with Pt.

Analysis of the fluorescence excitation and emission spectra identified two main spectral components. For this analysis, the mixture was activated for a relatively long time of 24 h to ensure a lack of **Cbz-PDI**. After the removal of TEA by evaporation, the major component with the absorption and fluorescence excitation band at 450 nm showed a fluorescence emission with a pronounced vibronic structure centered at 500 nm (Fig. 3C and D). The second minor component appeared in the absorption spectrum as a low-intensity tail; its fluorescence excitation spectrum had broad bands with an apparent maximum at 480 nm. This second component could be individually excited with a 500–550 nm light, which gave rise to a broad, structureless emission band centered at 590 nm. This emission was detected for a relatively long time (>100 ns) (Fig. 3E, Table 2).

As our attempts to isolate the activated species from the photocatalytic mixture using column chromatography and HPLC were unsuccessful, we further used LCMS analysis performed directly on the same mixture activated for 24 h. Two mass components were identified. In spite of the long activation time and lack of **Cbz-PDI** in the absorption spectra, a significant amount of a component with a mass peak of 1097.50 *m*/*z*, identical to the initial compound, was detected (Fig. S1 and S2, ESI†). This behavior can indicate the reverse transformation of the activated species back to **Cbz-PDI**, probably under the conditions of the chromatographic analysis. The second component had a peak at 1518.42 *m*/*z* corresponding to **Cbz-PDCA-Pt$_2$**, the structure of which is shown in Fig. 3F. This shows that platinum atoms are directly incorporated into the structure of the activated species forming an organometallic complex, explaining the origin of the photocatalytic activity in the HER.

To understand the mechanism of formation of **Cbz-PDCA-Pt$_2$**, we performed DFT calculations for the thermodynamics of the possible stages of transformation starting from **Cbz-PDI**, as depicted in Scheme 1. The opening of the first cyclic diamide starts with the nucleophilic attack of a hydroxyl anion on the carbonyl group, thus forming an anion localized on the amide nitrogen atom (from **Cbz-PICA-aN**). Such a species further transforms to a more stable tautomeric form with the charge localized on the oxygen atom (**Cbz-PICA-aO**) *via* intramolecular proton transfer, resulting in a decrease in the total Gibbs free energy of −301 kJ mol^{-1}. **Cbz-PICA-aO** coexists in dynamic equilibrium with its neutral protolytic form **Cbz-PICA-n**.

There are two possibilities of further transformations of **Cbz-PICA**. According to the first, in the synchronous mechanism marked by blue arrows in Scheme 1, another nucleophilic attack of a hydroxyl anion on **Cbz-PICA-aO** and opening of the second ring occurs in a similar way as described above with the formation of the dianion **Cbz-PDCA-daO** and a −103 kJ mol^{-1} decrease in Δ*G*. Protolytic equilibrium affords the neutral form of **Cbz-PDCA-n**, which can react with two equivalents of K_2PtCl_4 to give **Cbz-PDCA-Pt$_2$** with a total Δ*G* of −442 kJ mol^{-1}. Another possibility, marked by green arrows in Scheme 1, is the formation of a mononuclear complex **Cbz-PICA-Pt** *via* the reaction of **Cbz-PICA-n** with one equivalent of K_2PtCl_4 (Δ*G* = −216 kJ mol^{-1}), followed by basic hydrolysis of the cyclic diamide in **Cbz-PICA-Pt** (Δ*G* = −294 kJ mol^{-1}) and further reaction with K_2PtCl_4 (Δ*G* = −226 kJ mol^{-1}) to give **Cbz-PDCA-Pt$_2$**.

Interestingly, the neutral forms with open ring(s) (**Cbz-PICA-n**, **Cbz-PDCA-n**, and **Cbz-PDCA-Pt-n**) easily lose water, transforming back to closed-ring species. This makes the hydrolysis stages reversible in the absence of platinum, especially in neutral and acidic media, where considerable amounts of such neutral forms are present. In fact, such a feature of the 3-carboxamide-4-carboxyl perylene derivatives was applied recently for the preparation of PDI derivatives under mild conditions at room temperature.[25] The reversibility of the above mentioned hydrolysis stages explains the lack of activation of **Cbz-PDI** under irradiation in the absence of TEA and K_2PtCl_4. The Pt^{2+} dication(s) stabilize the ring-opened form(s), affording an organometallic complex. The reversibility of the hydrolysis of **Cbz-PDI** may be also one of the reasons for the difficulties in isolating **Cbz-PDCA-Pt$_2$**. In such a case, the *in situ* formation of **Cbz-PDCA-Pt$_2$** described here seems to be the most optimal way of preparing such an HER-active molecular catalyst.

While both of the above mentioned pathways are thermodynamically allowed, the experimental data indirectly support the first synchronous mechanism. Taking into account the results of analyses described above, we assume that the main component of the activated solution is **Cbz-PDCA** with both diamide cycles cleaved. The absorption and emission of such species should have a maxima close to those of perylene and band shape with a pronounced vibronic structure. Reverse cyclization under the conditions of the LCMS spectrum should yield **Cbz-PDI**, as in fact was discussed above. Moreover, the frontier molecular orbitals of **Cbz-PDCA** are localized on perylene (Fig. S3, ESI†), explaining the vibronic structure of the electronic spectra of the observed band at 450 nm. The second component of the activated mixture is thus **Cbz-PDCA-Pt$_2$**, with broad absorption and emission bands in the long-wavelength region due to the metal–ligand charge-transfer nature of the lowest energy transitions (Fig. S3, ESI†). It should be mentioned that more allowed electronic transitions responsible for the absorption of **Cbz-PDCA-Pt$_2$** have a similar energy to **Cbz-PDCA** as they are also localized on perylene (Fig. S3, ESI†).

Table 2 Spectral parameters and emission lifetimes of Cbz-PDI and Cbz-PDCA-Pt$_2$ in aqueous SDS solutions[a]

Compound	*c*(TEA) [M]	λ_{abs} [nm]	ε [M^{-1} cm^{-1}]	λ_{em} [nm]	τ_{PF} [ns]	τ_{DF} [μs]
Cbz-PDI	0	545	16 550	750	1.6	1.1
	0.3	545	16 550	750	0.7	—
Cbz-PDCA-Pt$_2$	0	450	10 250	695	4.2	—
	0.3	450	10 250	695	1.6	—

[a] λ_{abs}, λ_{em} – wavelength of absorption and emission maxima, respectively; ε – molar extinction coefficient; τ_{PF}, τ_{DF} – lifetimes of prompt (PF) and delayed (DF) fluorescence, respectively, monitored at the respective emission bands.

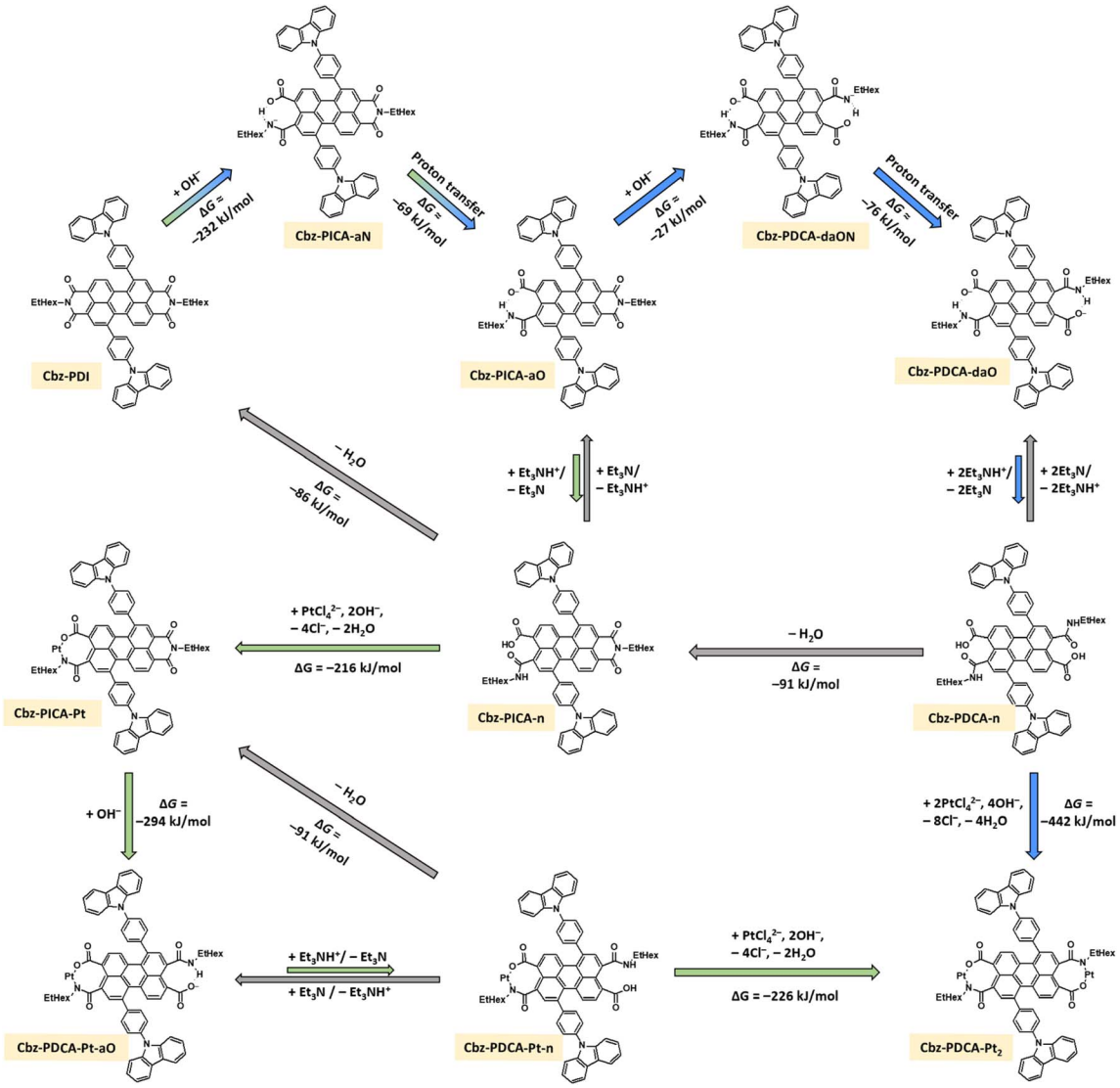

Scheme 1 Proposed mechanisms for the **Cbz-PDCA-Pt$_2$** formation in the presense of TEA. The green arrows indicate the stepwise mechanism, the blue arrows indicate the synchronous mechanism and the gray arrows indicate reverse transformations in neutral or acidic media.

HER performance

Optimization of the composition of the photocatalytic mixture. To estimate maximum HER efficiency of the developed photocatalytic system, HER tests were performed under various conditions, changing the concentrations of the mixture components and activation conditions.

To optimize the micellar photocatalytic system, the influence of SDS concentration was analyzed first (Fig. S4A, ESI†). We found that, due to low solubility, **Cbz-PDI** is not activated without SDS or when its concentration is below 1 mM. The optimum SDS concentration was found to be close to 2.1 mM, while systems with higher values showed a lower TON for the HER.

The molar ratio of **Cbz-PDI** and Pt is the key parameter for the investigated system. Fortunately, from the point of view of attempts to minimize the use of precious platinum, the maximum TON values were achieved with a much smaller ratio than that suggested by the **Cbz-PDCA-Pt$_2$** stoichiometry (1 : 2). In contrast, the use of a **Cbz-PDI** concentration of 80 μM and c(Pt) = 5 μM in a 16 : 1 molar ratio forty times higher than that suggested by the stoichiometry of the complex facilitated the activation procedure in terms of reaching the maximum intensity of the 450 nm absorption band more rapidly (Fig. 4A and B) and enabled a stable TOF value of 35 TON/h for the first 8 hours of irradiation after the addition of AA (Fig. 4C). Such experiments with an increased concentration of **Cbz-PDI** revealed that it is not completely degraded under these activation conditions, even after hours of irradiation. In fact, some remaining amounts of **Cbz-PDI** repeatedly detected in the absorption spectra of the activated mixture correlated with high, stable TOF values (Fig. 4B) and an estimated TON$_{24}$ of 800 (Table 3). The role of the remaining amounts of **Cbz-PDI** will be discussed further. Unfortunately, at such **Cbz-PDI** concentrations, the photocatalytic system is not stable due to the precipitation of large amounts of **Cbz-PDI**.

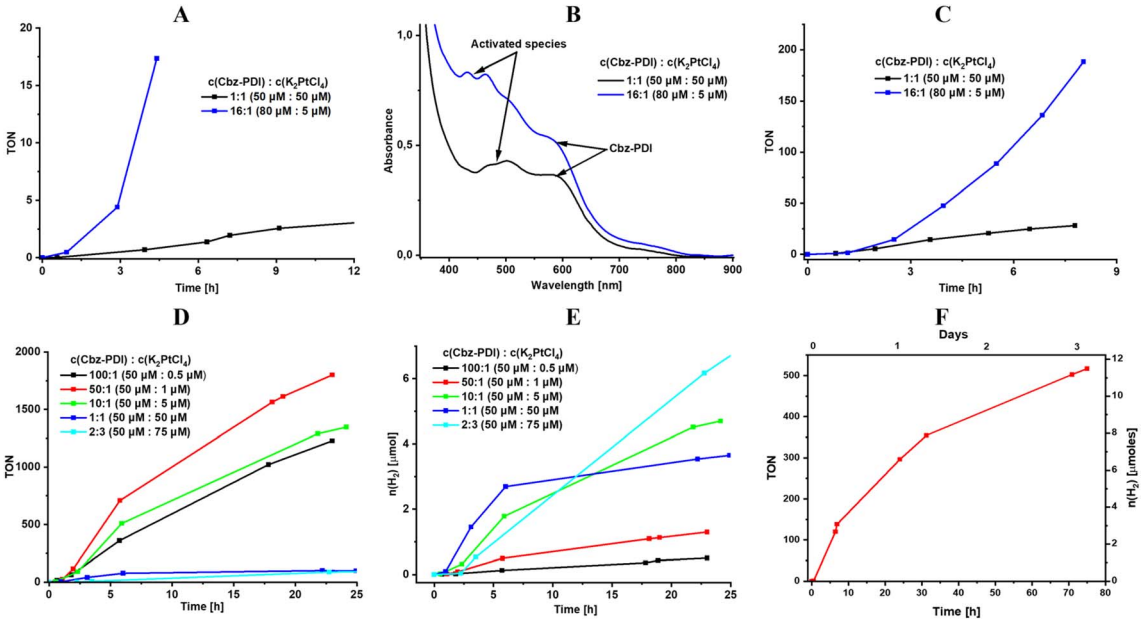

Fig. 4 HER tests on 3 mL solutions at 1 sun irradiation. Changes in the TON values (A) during activation with an excess of **Cbz-PDI** in the presence of TEA (0.3 M); absorption spectra (B) and HER performance (C) of the activated mixture containing AA (0.7 M). The HER performance of activated mixtures with various ratios of **Cbz-PDI** and Pt measured in TON (D) and number of moles of H_2 (E). HER stability test on 20 mL of solution (F).

To avoid deviations due to the uncontrolled precipitation of **Cbz-PDI**, we explored systems with a constant concentration of **Cbz-PDI** of 48 μM. The highest TON_{24} values, reaching 1900, were achieved in a mixture with an even larger molar ratio of 50 : 1 (Fig. 4D, Table 3), where the actual Pt concentration was 1 μM. Such a TON_{24} value calculated per mole of **Cbz-PDCA-Pt$_2$** is, however, underestimated because the **Cbz-PDCA-Pt$_2$** concentration is calculated assuming the complete complexation of Pt and not taking into account the losses during side-reactions. When the molar ratio was increased to 100 : 1 or decreased to 10 : 1, the TON_{24} value decreased to 1270 and 600, indicating an insufficient amount and less efficient utilization of Pt, respectively. The use of 1 : 1 and 2 : 3 molar ratios is almost one hundred times less efficient, indicating a high wastage of Pt, most likely due to the reduction and precipitation of metallic (nano)particles.

From the point of view of the actual amount of H_2 produced by the photocatalytic system, a 10 : 1 ratio seems to be the most optimum (Fig. 4E). A 3 mL volume of such a solution produces 4.6 μmol of H_2 in 24 h, which is only 1.4 times lower as compared to the mixture with a 1 : 2 ratio containing 20 times more Pt.

To estimate relatively long-term photoactivity of the **Cbz-PDCA-Pt$_2$** systems, an HER test was performed using an activated mixture of 50 μmol l^{-1} **Cbz-PDI**, 5 μmol l^{-1} K_2PtCl_4, 2.1 mM SDS, 0.3 M TEA and 0.7 M AA. The photoreaction was

Table 3 Photocatalytic parameters of the discussed HER experiments[a]

Test	$V_{sol.}$ [mL]	c(Cbz-PDI) [μM]	$c(K_2PtCl_4)$ [μM]	c(Cbz-PDI) : $c(K_2PtCl_4)$	c(AA) [M]	$n(H_2)_{24h}$ [μmol]	TON_{24h}	TOF_{max} [1/h]
1 (DMF)	3	50	0.5	100 : 1	0	<0.004	—	—
	3	50	50	1 : 1	0	0.05	14	0.7
2 (H_2O)	3	50	50	1 : 1	0	0.1 (19 h)	4 (19 h)	0.7
					0.7	0.8 (8 h)	28 (8 h)	6
	3	80	5	16 : 1	0	0.06 (4.5 h)	9 (4.5 h)	9
					0.7	4.3	800	43
3 (H_2O)	3	50	0.5	100 : 1	0.7	0.6	1270	197
	3	50	1	50 : 1	0.7	1.4	1900	157
	3	50	5	10 : 1	0.7	4.2	600	117
	3	50	50	1 : 1	0.7	3.4	100	18
	3	50	75	2 : 3	0.7	6.3	90	6
4 (H_2O)	21	50	5	10 : 1	0	6.5	280	13
					0.7	12.1	520	42

[a] Conditions: test 1 was performed in DFM with addition of 6.5% of H_2O without SDS, c(TEA) = 0.3 M; tests 2–4 were performed in water, c(SDS) = 2.1 mM, c(TEA) = 0.3 M.

carried out in a 43 mL reactor using 20 mL of the photocatalytic mixture. Under such conditions, more than 12 μmol of H_2 were produced within 3 days and the photocatalytic activity remained as high as $TOF_{72h} = 7\ h^{-1}$, which is a 43% decrease compared to that during the first 24 h (Fig. 4F). Cycle tests revealed gradual photobleaching and a three-fold decrease in the photocatalytic activity when irradiated with a full sunlight spectrum (Fig. S4C, ESI†). In contrast, when the UV light was optically filtered and only the >400 nm light was used for irradiation, the samples showed an impressively high quantitative stability of TOF = 5 h^{-1} for at least 3 days and significantly decreased photobleaching (Fig. S4C, ESI†).

In an attempt to analyze the activity of the **Cbz-PDCA-Pt$_2$** molecular catalyst in a soluble form without micellar support, we performed activation and HER tests on dimethylformamide with the addition of 6.5% (v/v) H_2O and 0.3 M TEA as a sacrificial electron donor. The activated mixtures showed similar changes in the absorption spectra as described earlier for the water–SDS medium but much lower activity. The activated mixture with a 1 : 1 molar ratio of **Cbz-PDI** and Pt afforded 50 nmol of H_2 in 24 h ($TON_{24h} = 14$, Table 3), whereas the activity of the mixture with a 100 : 1 ratio was below the detection limit of the chromatographic method used (4 nmol H_2). In contrast to the micellar nanoparticle medium where the reverse tendency was observed, this proved that the molecular catalyst was formed and was HER-active itself, but its performance in the dissolved form was much lower than in combination with a nanoparticle system, which correlates well with previous reports on Pt complexes.[26]

Suggested mechanism of the photocatalytic HER. The analysis of the computational investigations revealed that the LUMO energy of **Cbz-PDCA-Pt$_2$** was −4.26 eV. The HOMO energy was less than −5.5 eV, which is lower than that for the SEDs used: −5.13 eV (TEA) and −4.90 (AA),[27] enabling the formation of radical anionic species of **Cbz-PDCA-Pt$_2$** after the absorption of light. The emission quenching in the presence of SEDs supports this suggestion (Fig. 3E). The energies of the frontier orbitals of **Cbz-PDCA-Pt$_2$** thus enable the reduction of water in the presence of SEDs. The thermodynamic calculations revealed negative Gibbs free energies for all the key steps of the HER (Fig. 5A). The protonation of the **Cbz-PDCA-Pt$_2$** anionic radical at the Pt atom occurs with $\Delta G = -439$ kJ mol^{-1} and the further release of $\frac{1}{2}H_2$ causes energy decrease by 38 kJ mol^{-1}.

The above mentioned improvement in the performance of the HER in the presence of residual **Cbz-PDI** indicates its role as an electron mediator, which facilitates the storage of the energy of sunlight and electrons before the reduction of water occurs on **Cbz-PDCA-Pt$_2$**. In fact, in SDS-stabilized nanoparticles, this compound exhibits thermally activated delayed fluorescence (TADF) (Fig. S5, ESI†). This phenomenon occurs in molecular donor–acceptor systems when the energies of the excited singlet and triplet states are close. In the PL decay, such compounds show a region of delayed fluorescence (DF), which originates from the upconversion of T_1 to S_1 and further light emission. The duration of DF thus indicates the timescale of the stability of the T_1 state and the ability to store excitons for such a period of time. The occurrence of TADF in **Cbz-PDI** is evidence for the relatively high stability of its excited states, whereas its DF lifetime of 1.1 μs (Table 2) indicates the storage of excitation energy for a few microseconds. According to the computational results, the HOMO energy of **Cbz-PDI** is −5.70 eV, which is appropriate for the reaction of excited **Cbz-PDI** with the SEDs used. In fact, as supported by the emission decay measurements, its excited state is effectively quenched by TEA with a rate constant of $7.2 \times 10^8\ s^{-1}$ (Fig. S5, ESI†), affording the anionic radical. Perylene diimides are also known for the relatively high stability of their anionic radical species[28] and good electron transporting features.[29] Like various inorganic semiconductors used as electron mediators in heterogeneous photocatalytic systems, **Cbz-PDI** acts as a reservoir of excitation and electronic energies. Taking into account the LUMO energy of **Cbz-PDI** of −3.83 eV, electron is further transferred to the molecular catalyst **Cbz-PDCA-Pt$_2$** with a sufficiently lower LUMO of −4.26 eV.

Last but not least, the broader absorption of **Cbz-PDI** enables more efficient harvesting of sunlight than **Cbz-PDCA-Pt$_2$** itself. The above-mentioned considerations are perfectly supported by the HER test performed under irradiation with a 550 nm long-pass optical filter in which the light was only absorbed by **Cbz-PDI** (Fig. S4B, ESI†). When corrected by the difference in absorbance, the >550 nm light yielded only half the amount of H_2 obtained with the full sunlight spectrum, even though the molecular catalyst was not excited directly. Therefore, as summarized in Fig. 5B, in the discussed systems, **Cbz-PDI** serves as a photosensitizer of the red portion of the spectrum and can store excitation and electronic energies.

The core–shell nanoparticle structure presented in Fig. 5B is supported by the analysis of TEM images. Due to low solubility, the initial solution consists of nanoparticles of **Cbz-PDI** in SDS micelles (Fig. S6, ESI†). During activation, only the surface of such nanoparticles can easily transform to **Cbz-PDCA-Pt$_2$**, whereas the core retains **Cbz-PDI**, which, due to the lack of contact with solution, is hardly activated. In the case of the most efficient photocatalytic systems obtained under activation with a molar ratio of **Cbz-PDI** and Pt from 10 : 1 to 100 : 1, the recorded TEM images with distinct, well-defined, round-shaped nanoparticles with diameters of 10–100 nm (mode near to 37.7 nm) (Fig. 5C and S6, ESI†). Importantly, the uniform and relatively intense coloration of such nanoparticles supports the assumption on the metalorganic nature of their surface. Such observations indicate that **Cbz-PDCA-Pt$_2$** formation occurs on the surface of the nanoparticles, supporting the ideal situation presented in Fig. 5B. When the concentrations of **Cbz-PDI** and Pt were equimolar, the TEM images showed round-shaped nanoparticles with various degrees of coloration (Fig. 5C and S6, ESI†). The weaker coloration of most of the nanoparticles mainly indicates their organic nature, probably due to the less efficient formation of **Cbz-PDCA-Pt$_2$**. However, their surfaces are covered with smaller black spots of metallic Pt nanoparticles, formed by the light-induced reduction of K_2PtCl_4 in the presence of TEA. In such a case, the platinum atoms of **Cbz-PDCA-Pt$_2$** probably serve as one of the centers of crystallization for the Pt nanoparticles. Such equimolar samples are thus inhomogeneous, with most of the platinum concentrated in separate or aggregated nanoparticles (Fig. 5C), which explains the above mentioned lower TON values calculated per mol of Pt.

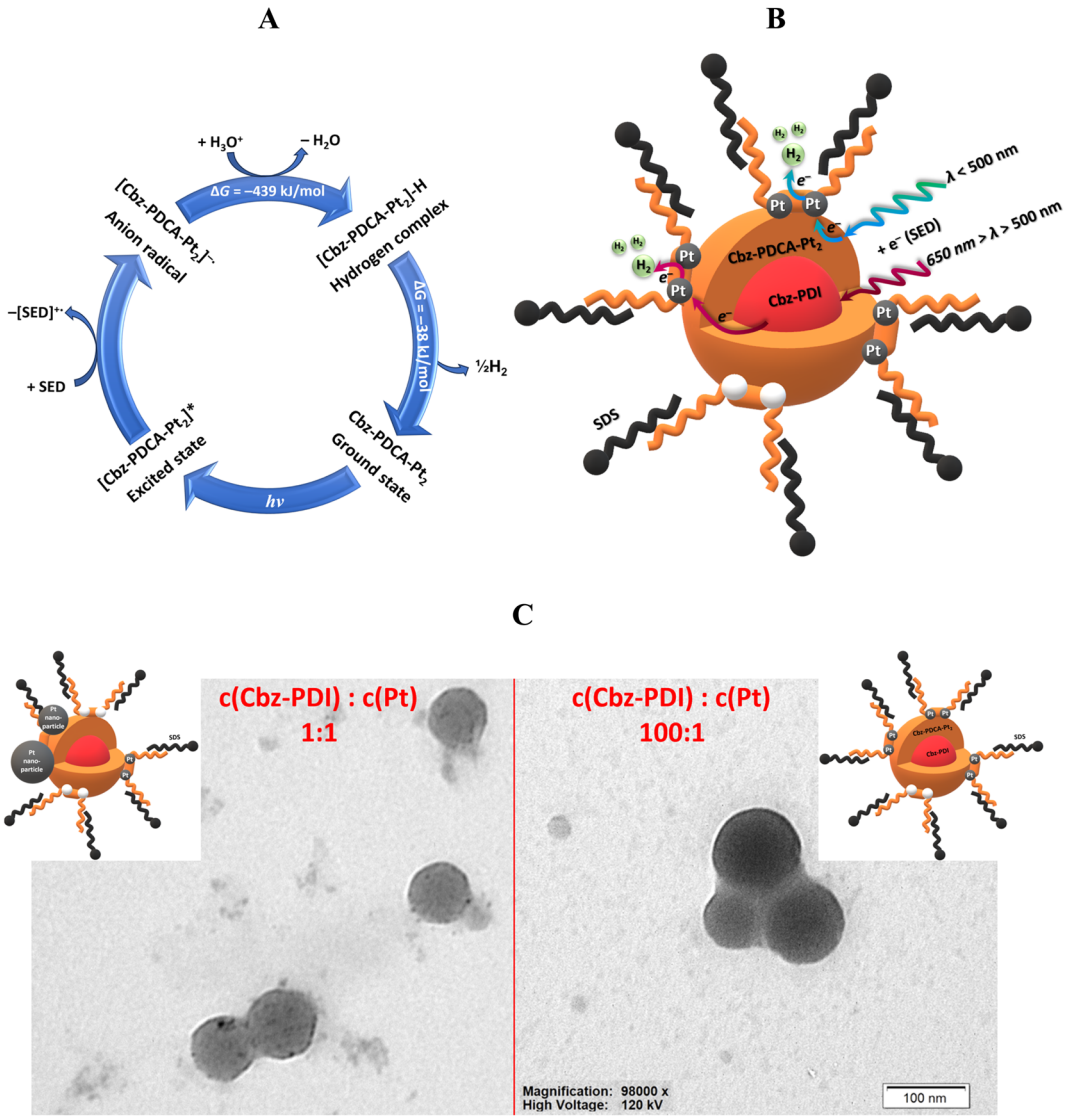

Fig. 5 The photocatalytic cycle of the **Cbz-PDCA-Pt$_2$** catalyst during HER (A). The suggested optimum structure of a photocatalytically active nanoparticle consisting of a **Cbz-PDI** core and **Cbz-PDCA-Pt$_2$** surface in SDS–water solutions (B). Comparison of the TEM images of two samples activated with different amount of Pt and the suggested structures of the nanoparticles (C).

According to the TEM images and absorption changes during activation experiments, the number of **Cbz-PDI** molecules and thus the size of the core varies depending on the initial concentration of **Cbz-PDI**. The **Cbz-PDCA-Pt$_2$** species represent the shell of the nanoparticles because they are formed on the surface in direct contact with the components of the solution. Depending on the amount of K_2PtCl_4 used, **Cbz-PDCA-Pt$_2$** can cover either all the surface of the nanoparticle, which is the ideal case or more realistically, only the part of the surface. The remaining ring-opened species **Cbz-PDCA** remain in a neutral or anionic form without platinum (Scheme 1). SDS molecules form a micelle around a core–shell nanoparticle. As mentioned above, very low concentrations of SDS are not enough to enable solubility of the photoactive nanoparticles, whereas high concentrations can block the access of the solution components to **Cbz-PDCA-Pt$_2$** on the surface and thus decrease the long-term photocatalytic efficiency.

Conclusions

In summary, the light-assisted cleavage of amide bonds in the perylene diimide derivative **Cbz-PDI** was discovered. In the presence of a platinum salt and triethylamine, the resulting bidentate ligand forms an organometallic complex **Cbz-PDCA-Pt$_2$** that acts as a photocatalyst in the hydrogen evolution reaction. The formation of this complex is accompanied by a blue shift in the absorption spectra due to a decrease in the electron-withdrawing strength of the perylene diimide acceptor. Taking into account the problematic isolation of **Cbz-PDCA-Pt$_2$** due to its low chemical stability under ambient conditions, the described *in situ* formation of this species seems to be the most convenient way of preparing this molecular catalyst. Analysis of the thermodynamics provided by the DFT calculations and experimental data indicated the formation of a bidentate ligand **Cbz-PDCA**, which, on further reaction with two equivalents of K_2PtCl_4, afforded **Cbz-PDCA-Pt$_2$**,

rather than a stepwise mechanism *via* a single-ring opening reaction and the formation of a mononuclear platinum complex. To the best of our knowledge, this is the first report of the light-induced formation of perylene-based organometallic compounds, opening a new direction for molecular photocatalysts in various applications.

The use of a mixture of **Cbz-PDCA-Pt$_2$** and **Cbz-PDI** in the HER tests afforded photocatalytic systems with the TON_{24h} exceeding 1900, economical use of platinum down to 10 molar percent, and retention of 67% of the photocatalytic stability after 3 days of HER performance. When calculated per unit mass of the active catalyst, one of the most efficient mixtures, containing 2 molar percent of Pt, afforded a hydrogen production rate of 30 mmol g^{-1} h^{-1} during the first 5 h and produced over 370 mmol g^{-1} H_2 after 24 h. This is higher than the efficiencies reported for other perylene-based systems, like *N*-annulated perylene diimide with platinized polymeric carbon nitride catalyst (12 mmol g^{-1} h^{-1}),[30] perylene diimide on palladium quantum dots (29 mmol g^{-1} h^{-1})[31] and self-assembled phosphoric acid substituted perylene diimide (11.7 mmol g^{-1} h^{-1}).[32] In contrast, a higher hydrogen production rate of 61 mmol g^{-1} h^{-1} was reported for nitrogen bay-annulated perylene diimide supramolecular photocatalysts,[33] indicating a promising pathway for further improvements in **Cbz-PDCA-Pt$_2$** systems.

Our results also indicate that the stability and microsecond lifetime of the excited states of **Cbz-PDI** are beneficial for the photocatalytic activity of the system. In general terms, the organic materials showing thermally activated delayed fluorescence can serve as electron mediators and excitation energy storage materials for applications in (photo)catalysis. In terms of stability, **Cbz-PDCA-Pt$_2$** and **Cbz-PDCA-Pt$_2$/Cbz-PDI** systems exceed the reported photocatalytic activity of other Pt(II) complexes more than 10 times,[20] which usually lose their activity after 6–8 h. The TON values achieved are also very high, although comparison with previous reports is complicated due to the different conditions used and lack of TON parameters in most of the reports.

Undoubtedly, the described molecular photocatalyst and its heterogenous mixture with **Cbz-PDI** needs further improvement. Further attempts will focus on the complexation with different metals, improvement of sunlight absorption, and solubility.

Experimental and computational methods

Sample preparation for spectroscopic measurements

Absorption and emission spectra of **Cbz-PDI** and **Cbz-PDCA-Pt$_2$** molecules were investigated in water micelles and/or in organic solvents as mentioned above. Water micelles were prepared by the addition of 20 μM of a 1 mM THF solution of a compound in 2.5 mL of a 0.01 M SDS water solution under sonication. The UV-Vis absorption spectra were recorded using a Shimadzu UV-1900 spectrophotometer. Steady-state photoluminescence spectra were recorded using an FS5 spectrofluorometer (Edinburgh Instruments).

Time-resolved emission spectra and emission decays were investigated using a customized system[34] consisting of a pulsed YAG:Nd laser (PL2251A, EKSPLA) coupled with an optical parametric generator (PG 401/SH) as the excitation light source and 2501S grating spectrometer (Bruker Optics) combined with a streak camera system (C4334-01 Hamamatsu) as the detection unit. These measurements provided the time-wavelength-intensity 3D matrices from which the decay of the emission band(s) was analyzed (for more details, see ESI†).

Sample preparation for Cbz-PDI activation and HER tests

Activation and photocatalytic tests were performed under irradiation with a sun simulator SCIENCETECH SF-300-A equipped with an airmass filter AM1.5 G enabling a light intensity of 1 sun at the sample surface. Samples for the hydrogen evolution reaction were prepared in the following manner. First, an appropriate amount of the 1 mM **Cbz-PDI** in THF solution was added dropwise under sonication to the 0.01 M SDS solution in water and the mixture was sonicated for 5 min. Next, an appropriate amount of the 1 mM K_2PtCl_4 solution in water was added, followed by the addition of an appropriate amount of TEA to achieve a 0.3 M solution. The mixture was placed into a reactor with a silicon septum and air was replaced with argon. The mixture was irradiated by simulated sunlight at 35–40 °C with continuous stirring for the activation of **Cbz-PDI** and formation of **Cbz-PDCA-Pt$_2$**. Depending on the amount of contamination of the solution and mixture, complete activation was achieved in 3 h to 24 h.

For target HER tests, ascorbic acid was added to the activated mixture up to a concentration of 0.7 M. Air was replaced with argon and the mixture was irradiated with simulated sunlight.

Calculations of parameters of the photocatalytic reaction

The amount of hydrogen produced was determined using a gas chromatograph GC-2030 (Shimadzu) with a BID detector calibrated using a gas mixture containing 0.092% H_2.

The production of one H_2 molecule requires two photocatalytic cycles. Therefore, unless otherwise stated, the turnover number (TON) describing the number of cycles that occurred on a catalyst is given by eqn (1):

$$\mathrm{TON} = 2\, n(\mathrm{H_2})/n(\textbf{Cbz-PDCA-Pt$_2$}), \quad (1)$$

where $n(H_2)$ is the number of moles of hydrogen in the gaseous phase and n(**Cbz-PDCA-Pt$_2$**) is the number of moles of the molecular catalyst estimated proportional to $n(K_2PtCl_4)/2$.

The rate of change of TON in a period of time, (Δt) and the turnover frequency (TOF), is given by eqn (2):

$$\mathrm{TOF} = \Delta\mathrm{TON}/\Delta t. \quad (2)$$

Quantum chemical calculations

Unconstrained geometry optimizations were carried out for individual species at ground state using the B3LYP[35] hybrid functional and Lan-L2DZ basis set implemented in the

Gaussian 16 program package.[36] The energies of the molecular orbitals and electronic transitions were available from the single-point calculations calculated for optimal ground state geometries.

Conflicts of interest

There are no conflicts to declare.

Acknowledgements

Financial support within the LIDER XI grant LIDER/47/0190/L-11/19/NCBR/2020 of the National Centre for Research and Development (NCBR), Poland is gratefully acknowledged. The quantum chemical calculations were performed on computers at the Wroclaw Centre for Networking and Supercomputing (WCSS), Poland.

References

1 Commission Delegated Regulation (EU) 2023/1185, *Off. J. Eur. Union*, L 157/20, 2023.
2 A. Wolf and N. Zander, *Inter Econ.*, 2021, **56**, 316.
3 X. Chen, S. Shen, L. Guo and S. S. Mao, *Chem. Rev.*, 2010, **110**, 6503.
4 B. Zhang and L. Sun, *Chem. Soc. Rev.*, 2019, **48**, 2216.
5 Y. Zhang, Y.-J. Heo, J.-W. Lee, J.-H. Lee, J. Bajgai, K.-J. Lee and S.-J. Park, *Catalysts*, 2018, **8**, 655.
6 J. Zhu, L. Hu, P. Zhao, L. Y. S. Lee and K.-Y. Wong, *Chem. Rev.*, 2020, **120**, 851.
7 K. Maeda, *J. Photochem. Photobiol., C*, 2011, **12**, 237.
8 B. Mondal, K. Sengupta, A. Rana, A. Mahammed, M. Botoshansky, S. G. Dey, Z. Gross and A. Dey, *Inorg. Chem.*, 2013, **52**, 3381.
9 Y. Han, H. Fang, H. Jing, H. Sun, H. Lei, W. Lai and R. Cao, *Angew. Chem., Int. Ed.*, 2016, **55**, 5457.
10 H. Lei, H. Fang, Y. Han, W. Lai, X. Fu and R. Cao, *ACS Catal.*, 2015, **5**, 5145.
11 U. J. Kilgore, M. P. Stewart, M. L. Helm, W. G. Dougherty, W. Scott Kassel, M. Rakowski DuBois, D. L. DuBois and R. Morris Bullock, *Inorg. Chem.*, 2011, **50**, 10908.
12 M. P. Stewart, M.-H. Ho, S. Wiese, M. L. Lindstrom, C. E. Thogerson, S. Raugei, R. Morris Bullock and M. L. Helm, *J. Am. Chem. Soc.*, 2013, **135**, 6033.
13 B. E. Conway and G. Jerkiewicz, *Electrochim. Acta*, 2000, **45**, 4075.
14 S. K. Lakhera, A. Rajan, T. P. Rugma and N. Bernaurdshaw, *Renewable Sustainable Energy Rev.*, 2021, **152**, 111694.
15 M. M. Quintanilha, B. A. Schimitd, A. M. F. Costa, D. H. Nakahata, D. de Alencar Simoni, J. C. T. Clavijo, D. H. Pereira, A. C. Massabni, W. R. Lustri and P. P. Corbi, *J. Mol. Struct.*, 2021, **1236**, 130316.
16 F. Lakadamyali and E. Reisner, *Chem. Commun.*, 2011, **47**, 1695.
17 P. Tang, H. J. Lee, K. Hurlbutt, P.-Y. Huang, S. Narayanan, C. Wang, D. Gianolio, R. Arrigo, J. Chen, J. H. Warner and M. Pasta, *ACS Catal.*, 2022, **12**, 3173.
18 C. Li, Z. Chen, H. Yi, Y. Cao, L. Du, Y. Hu, F. Kong, R. K. Campen, Y. Gao, C. Du, G. Yin, I. Y. Zhang and Y. Tong, *Angew. Chem., Int. Ed.*, 2020, **59**, 15902.
19 P. Du, J. Schneider, P. Jarosz and R. Eisenberg, *J. Am. Chem. Soc.*, 2006, **128**, 7726.
20 F. Wang, W.-G. Wang, H.-Y. Wang, G. Si, C.-H. Tung and L.-Z. Wu, *ACS Catal.*, 2012, **2**, 407.
21 K. Sakai and H. Ozawa, *Coord. Chem. Rev.*, 2007, **251**, 2753.
22 C. Wang, Y. Chen and W.-F. Fu, *Dalton Trans.*, 2015, **44**, 14483.
23 E. J. L. McInnes, R. D. Farley, C. C. Rowlands, A. J. Welch, L. Rovatti and L. J. Yellowlees, *J. Chem. Soc., Dalton Trans.*, 1999, 4203.
24 A. Keerthi and S. Valiyaveettil, *J. Phys. Chem. B*, 2012, **116**, 4603.
25 M. C. Kwakernaak, M. Koel, P. J. L. van den Berg, E. M. Kelder and W. F. Jager, *Org. Chem. Front.*, 2022, **9**, 1090.
26 G. Li, M. F. Mark, H. Lv, D. W. McCamant and R. Eisenberg, *J. Am. Chem. Soc.*, 2018, **140**, 2575.
27 Y. Pellegrin and F. Odobel, *C. R. Chim.*, 2017, **20**, 283.
28 J. Cann, B. S. Gelfand and G. C. Welch, *Mol. Syst. Des. Eng.*, 2020, **5**, 1181.
29 V. Sharma, J. D. B. Koenig and G. C. Welch, *J. Mater. Chem. A*, 2021, **9**, 6775.
30 F. Yu, Z. Wang, S. Zhang, K. Yun, H. Ye, X. Gong, J. Hua and H. Tian, *Appl. Catal., B*, 2018, **237**, 32.
31 Y. Li, X. Zhang and D. Liu, *J. Photochem. Photobiol.*, 2021, **48**, 100436.
32 K. Kong, S. Zhang, Y. Chu, Y. Hu, F. Yu, H. Ye, H. Dinga and J. Hua, *Chem. Commun.*, 2019, **55**, 8090.
33 H. Xu, Z. Wang, S. Feng, X. Liu, X. Gong and J. Hua, *Int. J. Hydrogen Energy*, 2023, **48**, 8071.
34 A. A. Kubicki, P. Bojarski, M. Grinberg, M. Sadownik and B. Kukliński, *Opt. Commun.*, 2006, **269**, 275.
35 A. D. Becke, *J. Chem. Phys.*, 1993, **98**, 1371.
36 M. J. Frisch, G. W. Trucks, H. B. Schlegel, G. E. Scuseria, M. A. Robb, J. R. Cheeseman, G. Scalmani, V. Barone, G. A. Petersson, H. Nakatsuji, X. Li, M. Caricato, A. V. Marenich, J. Bloino, B. G. Janesko, R. Gomperts, B. Mennucci, H. P. Hratchian, J. V. Ortiz, A. F. Izmaylov, J. L. Sonnenberg, D. Williams-Young, F. Ding, F. Lipparini, F. Egidi, J. Goings, B. Peng, A. Petrone, T. Henderson, D. Ranasinghe, V. G. Zakrzewski, J. Gao, N. Rega, G. Zheng, W. Liang, M. Hada, M. Ehara, K. Toyota, R. Fukuda, J. Hasegawa, M. Ishida, T. Nakajima, Y. Honda, O. Kitao, H. Nakai, T. Vreven, K. Throssell, J. A. Montgomery Jr, J. E. Peralta, F. Ogliaro, M. J. Bearpark, J. J. Heyd, E. N. Brothers, K. N. Kudin, V. N. Staroverov, T. A. Keith, R. Kobayashi, J. Normand, K. Raghavachari, A. P. Rendell, J. C. Burant, S. S. Iyengar, J. Tomasi, M. Cossi, J. M. Millam, M. Klene, C. Adamo, R. Cammi, J. W. Ochterski, R. L. Martin, K. Morokuma, O. Farkas, J. B. Foresman and D. J. Fox, *Gaussian 16, Revision C.01*, Gaussian, Inc., Wallingford CT, 2016.